QUARTERLY OF APPLIED MATHEMATICS
VOLUME LXXIV, NUMBER 3
SEPTEMBER 2016, PAGES 399–420
http://dx.doi.org/10.1090/qam/1423
Article electronically published on June 16, 2016

ON THE STABILITY OF AN ELLIPSOIDAL TUMOUR

By

GEORGE DASSIOS (*Department of Chemical Engineering, University of Patras and FORTH/ICE-HT, Greece*)

AND

VASILIKI CHRISTINA PANAGIOTOPOULOU (*Department of Chemical Engineering, University of Patras and FORTH/ICE-HT, Greece*)

Abstract. The ellipsoid represents the sphere of the anisotropic space. It provides the appropriate geometrical model for any direction dependent physical quantity. The growth of a tumour does depend on the available tissue surrounding the tumour, and therefore it represents a physical case which is realistically modelled by ellipsoidal geometry. Such a model has been analysed recently by Dassios et al. (2012). In the present work, we focus on the stability of the growth of an ellipsoidal tumour. It is shown that, in contrast to the highly symmetric spherical case, where stability can possibly be achieved, there are no conditions that secure the stability of an ellipsoidal tumour. Hence, as in many physical cases, the observed instability is a consequence of the lack of symmetry.

1. Introduction. Cancer cells are a result of genetic mutations of normal cells. Tumour colonies obtain their nutrients (oxygen and glucose) and extract waste products in a similar fashion as the other non-cancerous cells via simple diffusion. At these early stages, the tumour increases at an exponential rate ([34]), since all cells are well-nourished and proliferate at their highest rate possible, as supported by the work of [14]. During the early stages of tumour tissue development, the nutrients are in abundance; thus the proliferation rate is maximal and the rate of tumour growth is exponential.

As the colony increases in size, oxygen concentration near the tumour centre decreases, since the nutrients are consumed en route from the outside to the inside of the tumour. The proliferation rate of central cells is gradually reduced. Further reduction in the oxygen concentration below a threshold value, especially oxygen, reversibly arrests cell proliferation, and the non-dividing cells remain alive (see [28]). The cells with arrested proliferation are known as quiescent, and they can recover to proliferating cells once the nutrient supply is restored.

Received October 3, 2014.
2010 *Mathematics Subject Classification.* Primary 92B05, 42C10, 33E10, 33E05, 34B60, 34D10, 53Z05, 65L10.
E-mail address: gdassios@otenet.gr
E-mail address: vpanagi@chemeng.upatras.gr

As the tumour increases in size further, the concentrations of nutrients fall even more. Once they reach a second threshold value, the cells in the centre cannot support their basic metabolic needs and eventually die, forming a collection of necrotic tissue.

A tumour cross-section consists of an outer zone of fully proliferating cells, an intermediate zone of quiescent cells and a central core of necrotic tissue and cell debris ([30]), as depicted schematically in Figure 1. Once these three regions are formed, the outer zone remains constant in size. Every new layer of cells on the outside of the outer ring is accompanied by a newly formed layer of quiescent cells at the intermediate zone interface. As the tumour continues to develop, the rim of adequately nourished viable cells at the surface becomes roughly constant in size, leading to a phase of near linear growth, as suggested by [16], [29] and [7]. Eventually due to the diffusion-limited accumulation of nutrients and wastes, the action of necrotic disintegration, the mitotic inhibitory factors and the delayed proliferation rate, the tumour reaches a maximal size (see the work of [48], [27] and [35]). This dynamic steady state occurs when the death rate equals the proliferation rate, as supported by the work of [44], [9] and [37]. Experiments of *in vitro* growth of nodular carcinomas, which are described by [23] and [33], as well as those involving techniques for the *in vivo* isolation of tumours (see [24], [26] and [46]) support the hypothesis of the existence of a dormant but viable steady state described also in [25] and [45]. If we assume that this is a spherical-like configuration, its diameter measures only a few millimetres (around 2 mm as observed by [25]). This structure identifies an avascular tumour, which as the term implies, is a tumour without its own blood network. There are tumours that remain in the avascular stage indefinitely. However, under hy-

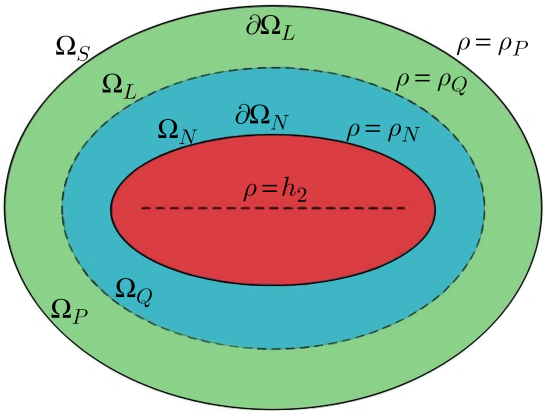

FIG. 1. Cross-section of the ellipsoidal tumour

poxic stimulation, most tumours exhibit the angiogenic tendencies. A brief description of angiogenesis tailor-made for mathematical analysis is found in the book written by [34]. Tumour angiogenesis is driven by hypoxia. The cancerous cells release tumour angiogenic factors (TAFs), a family of proteins that promote angiogenesis in tumours. An important member of TAFs is vascular endothelial growth factor (VEGF). VEGF acts on the neighbouring vasculature and promotes chemotactic and haptotactic angiogenesis ([1]). The result of VEGF action is the sprouting of capillary ends towards the tumour following

the VEGF gradient. Capillary tips that come into close proximity join together, forming anastomoses, through which circulating blood can flow. Secondary sprouts emanate from the new loops and so the process continues, with increasing numbers of capillary tips being formed until the new vessels penetrate the tumour. The newly formed vessels restore the nutrient supply, and the proliferation rate of the tumour increases. Now the tumour is characterized as vascular, and its size continues to grow beyond the size at the saturation level (steady state size), as described by [23].

The presence of blood vessels that connect the tumour with the adjacent vasculature does not only serve for the nourishment of the colony. Small clusters of tumour cells can detach from the original aggregation and travel to distant tissues via the blood network of the host. If the conditions in the new sites are favourable, they will establish secondary tumours or metastases that further weaken the host (see [49]). When that happens, the tumour has reached the metastatic phase. Moreover, the rapid growth of vascular tumours may impair the function of neighbouring organs. Invasion is another key characteristic of tumours. Byrne et al. [9] suggest that contact with the surrounding tissue stimulates the production of enzymes that digest the tissue, liberating space into which the tumour cells migrate.

Greenspan [31] was the first to model surface perturbation on an initially spherical tumour. The extensions and modifications to Greenspan's original model of multicellular spheroids (MCS) are now so numerous that it is impossible to do justice to them ([1], [43], [47] and [44]). Important developments include relaxing the assumption of radially symmetric growth ([1], [10] and [30]) and distinguishing different cell populations within the spheroid (see [49]). For example, while Greenspan [31] used analytical techniques to predict how the invasive boundary of a tumour initially develops, [18] used sophisticated numerical methods to solve the system of nonlinear equations and relate the irregular shapes adopted by the tumour to the values of key model parameters.

If the tumour is assumed to be an incompressible fluid and contains no voids or holes, then cell proliferation and death generate spatial variations in the pressure within the tumour which drive cell motion, with cells moving down pressure gradients, away from regions of net cell proliferation and toward regions of net cell death. Surface tension is also incorporated into the model as a mechanism for maintaining the compactness of the tumour and counteracting the expansive forces caused by cell proliferation ([8]). Byrne [8] presented an analysis that provided a mechanism which may explain how the irregular morphology characterising invasive tumours may be initiated. To understand this, Byrne [8] considered a uniform cluster of tumour cells for which the surface tension coefficient is significantly large then the underlying radially symmetric solution is linearly stable to symmetry-breaking perturbations, including the use of Legendre polynomials. This particular analysis predicted that such a cluster would remain radially symmetric through its development.

Suppose now that the cells undergo a transformation which weakens the surface tension forces holding the tumour cells together. If the reduction is significant, then the tumour will become unstable to a finite range of asymmetric perturbations and will develop an irregular morphology. Byrne [8] noted that similar quantitative behaviour is obtained if, instead of invoking surface tension (and the associated jump in the pressure across the

tumour boundary), the nutrient concentration is assumed to be discontinuous across the tumour boundary, with a jump related to the local curvature. The physical motivation for this boundary condition is that the nutrients (or their energy equivalents) are utilized by cells on the tumour boundary to maintain its compactness.

Avascular tumours that possess irregular boundaries have also been reported. In order to understand how such non-uniform boundaries may form, several authors have used linear techniques to investigate the stability of radially symmetric tumour configurations to asymmetric perturbations, the underlying spherically symmetric state resembling avascular nodules, as predicted by the work of [31], [15] and [10]. Recently, Byrne [5] has used weakly nonlinear analysis to resolve these problems. The researchers have studied the global stability of quasi-steady solutions for a simple mathematical model describing the growth of a spherical vascularised tumour consisting only of living cells. By assuming the rates of proliferation and absorption to be increasing nonlinear functions of the nutrient concentration, they establish the existence of a non-trivial steady solution and conditions for the existence and uniqueness of a quasi-steady solution for each initial configuration. Also, we prove that all these quasi-steady solutions converge uniformly to a non-trivial steady solution. The quasi-steady approach is justified by the smallness of the parameter that measures the ratio between the timescales for the diffusion of nutrients and growth of the tumour ([4]).

In our approach, we use the model proposed by Dassios et al. [21] for an ellipsoidal tumour colony. The approach of the cancer geometry as an ellipsoid is based on ultrasound images and other imaging techniques in patients with breast cancer ([50] and [2]) and cervical cancer [38], as well as in experiments *in vivo* [22] and in *in vitro* tumour cultures [39].

The present paper is organised as follows. In Section 2 one can find the equations and the conditions that are used for the ellipsoidal model. Section 3 refers to the unperturbed model proposed by [21], while Section 4 is devoted to the perturbed part. Section 5 summarises the results for both unperturbed and perturbed parts with numerical and graphical examples. A final Section 6 is used for discussion and future plans.

2. Stating the problem and introducing the equations for the model. To model an avascular tumour, we assume a three–layered structure for its interior cell distribution. In the centre of the tumour there is a necrotic core occupied by dead cells and debris. This core is enveloped by a quiescent layer of live but not proliferating cells (quiescent cells), whereas close to the tumour boundary there is a thin layer of live proliferating cells. For our approach we assume that all three layers are of ellipsoidal shape as part of the confocal ellipsoidal family with foci $(\pm h_2, 0, 0)$, $(\pm h_3, 0, 0)$, $(0, \pm h_1, 0)$. The ellipsoidal system is defined by

$$x_1 = \frac{\rho\mu\nu}{h_2 h_3}, \tag{2.1}$$

$$x_2 = \frac{\sqrt{\rho^2 - h_3^2}\sqrt{\mu^2 - h_3^2}\sqrt{h_3^2 - \nu^2}}{h_1 h_3}, \tag{2.2}$$

$$x_3 = \frac{\sqrt{\rho^2 - h_2^2}\sqrt{h_2^2 - \mu^2}\sqrt{h_2^2 - \nu^2}}{h_1 h_2}, \tag{2.3}$$

where (ρ, μ, ν) and (x_1, x_2, x_3) are the ellipsoidal and Cartesian coordinates respectively. The referenced ellipsoid is given by

$$\frac{x_1^2}{\alpha_1^2} + \frac{x_2^2}{\alpha_2^2} + \frac{x_3^2}{\alpha_3^2} = 1,\ 0 < \alpha_3 < \alpha_2 < \alpha_1 < \infty\ , \tag{2.4}$$

in Cartesian coordinates, where

$$h_1^2 = \alpha_2^2 - \alpha_3^2,\ h_2^2 = \alpha_1^2 - \alpha_3^2,\ h_3^2 = \alpha_1^2 - \alpha_2^2 \tag{2.5}$$

are the semi–focal distances.

The difference between the three areas of the tumour lies in the nutrient concentration σ. Cells proliferate while the nutrient concentration is larger than the critical level σ_1. A cell stays alive but does not proliferate when the nutrient supply remains over the critical level σ_2 and under σ_1. When the nutrient concentration falls under σ_2, the cell is found in the necrotic core. For that, we distinguish the tumour and its surroundings into four regions (Ω_N, Ω_Q, Ω_P, Ω_S). Ω_N denotes the ellipsoidal necrotic core, the ellipsoidal shell Ω_Q consists of quiescent cells, the ellipsoidal shell Ω_P hosts the proliferating cells and Ω_S stands for the area outside the tumour. In terms of nutrient concentration, the ellipsoidal regions are specified as

$$\Omega_N = \{(\rho, \mu, \nu) : h_2 \le \rho < \rho_N,\ \sigma(\boldsymbol{r}) < \sigma_2\}, \tag{2.6}$$

$$\Omega_Q = \{(\rho, \mu, \nu) : \rho_N < \rho < \rho_Q,\ \sigma_2 < \sigma(\boldsymbol{r}) < \sigma_1\}, \tag{2.7}$$

$$\Omega_P = \{(\rho, \mu, \nu) : \rho_Q < \rho < \rho_L,\ \sigma(\boldsymbol{r}) > \sigma_1\}, \tag{2.8}$$

$$\Omega_S = \{(\rho, \mu, \nu) : \rho > \rho_L,\ \sigma_1 < \sigma(\boldsymbol{r}) < \sigma_\infty\}, \tag{2.9}$$

where $\sigma(\boldsymbol{r})$ is the nutrient concentration at the point $\boldsymbol{r} = (\rho, \mu, \nu)$ and σ_∞ is the nutrient concentration from an exterior nutrient source that constantly supplies the tumour.

We assume that the nutrient concentration is in a diffusive steady state, so that

$$\Delta\sigma_i(\boldsymbol{r}) = 0\ , \boldsymbol{r} \in \Omega_i,\ i = N, L, S, \tag{2.10}$$

where $\sigma_N(\boldsymbol{r})$, $\sigma_L(\boldsymbol{r})$, $\sigma_S(\boldsymbol{r})$ denote the nutrient concentrations at the point $\boldsymbol{r}$ of Ω_N, $\Omega_L = \Omega_Q \cup \Omega_P$ and Ω_S respectively.

If we assume that the tumour is modelled by an incompressible fluid, changes in cell population will result in motion within the structure and thus in alterations in pressure distribution. This is expressed as

$$\Delta p = S_1 \mathcal{H}\left(|\boldsymbol{r}| - |\boldsymbol{r_N}|\right) + S_2 \mathcal{H}\left(|\boldsymbol{r}_N| - |\boldsymbol{r}|\right)\ , \tag{2.11}$$

where S_1 is the constant net rate of cell loss due to apoptosis in the living area (proliferating and quiescent layer) and S_2 is the cell loss rate because of necrosis in the necrotic core. $\mathcal{H}$ is the Heaviside step function and $\boldsymbol{r}_N$ denotes a point on the surface of the necrotic area. On the boundary of the necrotic core, $\partial\Omega_N$, we assume continuity for the nutrient concentration, the pressure distribution and its gradient:

$$\sigma_N(\boldsymbol{r}_N) = \sigma_L(\boldsymbol{r}_N)\ , \tag{2.12}$$

$$p_N(\boldsymbol{r}_N) = p_L(\boldsymbol{r}_N)\ , \tag{2.13}$$

$$\hat{\boldsymbol{n}} \cdot \nabla p_N\Big|_{\boldsymbol{r}=\boldsymbol{r}_N} = \hat{\boldsymbol{n}} \cdot \nabla p_L\Big|_{\boldsymbol{r}=\boldsymbol{r}_N}\ , \tag{2.14}$$

where p_N denotes the pressure in the necrotic region, p_L the pressure in the living layer and $\hat{\boldsymbol{n}}$ is the unit normal vector. On the boundary of the tumour $\partial\Omega_P$, the following conditions are dictated by the Greenspan model:

$$\hat{\boldsymbol{n}}\cdot\nabla\sigma_L\Big|_{\boldsymbol{r}=\boldsymbol{r}_L} = \frac{\gamma}{k}s(\boldsymbol{r}_L)\ , \tag{2.15}$$

$$\sigma_L(\boldsymbol{r}_L) = \sigma_S(\boldsymbol{r}_L)\ , \tag{2.16}$$

$$\frac{\mathrm{d}\boldsymbol{r}}{\mathrm{dt}}\cdot\hat{\boldsymbol{n}}\Big|_{\boldsymbol{r}=\boldsymbol{r}_L} = -\hat{\boldsymbol{n}}\cdot\nabla p\Big|_{\boldsymbol{r}=\boldsymbol{r}_L} + \frac{\beta}{d_t}s(\boldsymbol{r}_L)\ , \tag{2.17}$$

$$\frac{\mathrm{d}\boldsymbol{r}}{\mathrm{dt}}\times\hat{\boldsymbol{n}}\Big|_{\boldsymbol{r}=\boldsymbol{r}_L} = -\hat{\boldsymbol{n}}\times\nabla p_L\Big|_{\boldsymbol{r}=\boldsymbol{r}_L}\ , \tag{2.18}$$

where γ denotes the rate of mass/volume consumption, k the diffusion constant, β the mass/volume production, d_t the mass density of the tumour colony and $s(\boldsymbol{r}_L)=h_\rho^L(\rho_L-\rho_Q)$ is the local thickness. The latter parameter provides the key difference from the Greenspan approach, as instead of using a square root law we introduce the local thickness s. Note that h_ρ^L is one of the metric coefficients defined in Appendix B. Furthermore, on the outer boundary $\partial\Omega_P$, we assume that the pressure satisfies the Young–Laplace relation (see [20])

$$p_L(\boldsymbol{r}_L)-p_S(\boldsymbol{r}_L) = \alpha\kappa(\boldsymbol{r}_L)\ , \tag{2.19}$$

where $p_L(\rho_L)=g(\rho_L)$ and p_S denotes the pressure in the surrounding area of the tumour. As $|\boldsymbol{r}|\to 0$, p_N must be smooth. The source of nutrients is assumed to be constant far away from the tumour, that is,

$$\sigma_S=\sigma_\infty \text{ as } r\to\infty. \tag{2.20}$$

Following Greenspan's approach, we introduce a perturbation on the ellipsoidal coordinate ρ which is relevant to the radial coordinate of the spherical coordinate system. We are interested in perturbations of the outer tumour boundary, that is,

$$\rho(t)=\rho_L(t)+\varepsilon f(\mu,\nu,t)\ , \tag{2.21}$$

where ε is a small parameter and $f(\mu,\nu)$ is the spatial variable of the perturbed part depending on μ,ν, the angular coordinates of the ellipsoidal geometry, and on time. We introduce the same perturbation factor in the pressure distribution:

$$p_N = \bar{p}_N+\varepsilon\tilde{p}_N\ , \tag{2.22}$$

$$p_L = \bar{p}_L+\varepsilon\tilde{p}_L\ , \tag{2.23}$$

$$p_S = \bar{p}_S+\varepsilon\tilde{p}_S\ , \tag{2.24}$$

and in the nutrient concentration:

$$\sigma_N = \bar{\sigma}_N+\varepsilon\tilde{\sigma}_N\ , \tag{2.25}$$

$$\sigma_L = \bar{\sigma}_L+\varepsilon\tilde{\sigma}_L\ , \tag{2.26}$$

$$\sigma_S = \bar{\sigma}_S+\varepsilon\tilde{\sigma}_S\ , \tag{2.27}$$

where $\bar{p}_N,\ \bar{p}_L,\ \bar{p}_N,\ \bar{\sigma}_N,\ \bar{\sigma}_L,\ \bar{\sigma}_S$ are the variables of the ellipsoidal tumour, and $\tilde{p}_N,\ \tilde{p}_L,\ \tilde{p}_N,\ \tilde{\sigma}_N,\ \tilde{\sigma}_L,\ \tilde{\sigma}_S$ are the variables of the perturbed part. The same applies for the curvature of the outer boundary,

$$\kappa = \bar{\kappa} + \varepsilon\tilde{\kappa}\ , \tag{2.28}$$

and the interior pressure on the outer boundary,

$$g(\rho_L) = \bar{g}(\rho_L) + \varepsilon\tilde{g}(\rho_L). \tag{2.29}$$

3. Unperturbed part. For the unperturbed ellipsoidal part of the tumour, we obtain Laplace equations for the nutrient concentration in the necrotic core, the living layer and outside the tumour as

$$\Delta\bar{\sigma}_N = 0\ , \tag{3.1}$$

$$\Delta\bar{\sigma}_L = 0\ , \tag{3.2}$$

$$\Delta\bar{\sigma}_S = 0\ . \tag{3.3}$$

In this mode, we assume two different rates of cell death that translate into two different Poisson equations for the pressure distribution in the core of the tumour $\bar{p}_N$ and the shell of living layers $\bar{p}_L$, that is,

$$\Delta\bar{p}_N = S_1\ , \tag{3.4}$$

$$\Delta\bar{p}_L = S_2\ . \tag{3.5}$$

On the interface between the necrotic core and the living layer we assume continuity for the nutrient concentration, the pressure and its gradient:

$$\bar{\sigma}_N = \bar{\sigma}_L\ , \tag{3.6}$$

$$\bar{p}_N = \bar{p}_L\ , \tag{3.7}$$

$$\frac{\partial\bar{p}_N}{\partial\rho} = \frac{\partial\bar{p}_L}{\partial\rho}\ . \tag{3.8}$$

As for the outer tumour boundary, equations (2.15)-(2.17) imply

$$\frac{\partial\bar{\sigma}_L}{\partial\rho} = \frac{\gamma}{k}\left(h_\rho^L\right)^2(\rho_L - \rho_Q)\ , \tag{3.9}$$

$$\bar{\sigma}_L = \bar{\sigma}_S\ , \tag{3.10}$$

$$\left(h_\rho^L\right)^2\frac{\mathrm{d}\rho_L}{\mathrm{dt}} = -\frac{\partial\bar{p}_L}{\partial\rho} + \frac{\beta}{d_t}\left(h_\rho^L\right)^2(\rho_L - \rho_Q)\ . \tag{3.11}$$

Equation (2.18) represents the evolution of cells on the outer surface of the tumour and provides the following equations:

$$\left(h_\mu^L\right)^2\frac{\mathrm{d}\mu}{\mathrm{dt}} = \frac{\partial\bar{p}_L}{\partial\mu}\ , \tag{3.12}$$

$$\left(h_\nu^L\right)^2\frac{\mathrm{d}\nu}{\mathrm{dt}} = \frac{\partial\bar{p}_L}{\partial\nu}\ . \tag{3.13}$$

By assuming that

$$\bar{p}_L = \bar{g}(\rho_L)\ , \tag{3.14}$$

where $\bar{g}(\rho_L)$ is a function of ρ, constant on the boundary $\rho=\rho_L$, the exterior pressure on the outer boundary of the tumour is given by

$$\bar{p}_S=\bar{g}(\rho_L)-\alpha\bar{\kappa}\ . \tag{3.15}$$

The nutrient source uniformly supplies the tumour

$$\bar{\sigma}_S\to\sigma_\infty \text{ as } r\to\infty\ . \tag{3.16}$$

As in [21], the nutrient concentration within the necrotic region is given by

$$\begin{aligned}\bar{\sigma}_N=\sigma_2-\frac{\sigma_\infty-\sigma_2}{\Lambda-\Lambda'}\frac{I_2^1(\rho_N)}{I_0^1(\rho_N)}\frac{E_2^1(\rho)S_2^1(\mu,\nu)}{\frac{3}{2\pi}V(\rho_L)I_2^1(\rho_L)E_2^1(\rho_L)-1}\\ +\frac{\sigma_\infty-\sigma_2}{\Lambda-\Lambda'}\frac{I_2^2(\rho_N)}{I_0^1(\rho_N)}\frac{E_2^2(\rho)S_2^2(\mu,\nu)}{\frac{3}{2\pi}V(\rho_L)I_2^2(\rho_L)E_2^2(\rho_L)-1}\ ,\end{aligned} \tag{3.17}$$

where $I_n^m(x)$ are the elliptic integrals, $E_n^m(x)$ the Lamé functions and $S_n^m(\mu,\nu)$ the surface ellipsoidal harmonics, all of them defined in Appendix A. For the nutrient concentration outside the necrotic core, we obtain

$$\begin{aligned}\bar{\sigma}_L=\bar{\sigma}_S=\sigma_\infty-(\sigma_\infty-\sigma_2)\frac{I_0^1(\rho)}{I_0^1(\rho_N)}-\frac{\sigma_\infty-\sigma_2}{\Lambda-\Lambda'}\frac{I_2^1(\rho)}{I_0^1(\rho_N)}\frac{E_2^1(\rho)S_2^1(\mu,\nu)}{\frac{3}{2\pi}V(\rho_L)I_2^1(\rho_L)E_2^1(\rho_L)-1}\\ +\frac{\sigma_\infty-\sigma_2}{\Lambda-\Lambda'}\frac{I_2^2(\rho)}{I_0^1(\rho_N)}\frac{E_2^2(\rho)S_2^2(\mu,\nu)}{\frac{3}{2\pi}V(\rho_L)I_2^2(\rho_L)E_2^2(\rho_L)-1}\ .\end{aligned} \tag{3.18}$$

Next we state the expressions for the pressure distribution in the core of the tumour:

$$\begin{aligned}\bar{p}_N=&\left[\bar{g}(\rho_L)+(S_1-S_2)\frac{V(\rho_N)}{4\pi}I_0^1(\rho_N,\rho_L)+\frac{S_1}{6}\left(\rho_N^2-\rho_L^2\right)+\frac{S_2}{6}\left(\rho^2-\rho_N^2\right)\right]\\ &-\left[(S_1-S_2)\frac{V(\rho_N)}{4\pi}I_2^1(\rho_N,\rho_L)+\frac{S_1\left(\rho_N^2-\rho_L^2\right)}{6E_2^1(\rho_N)E_2^1(\rho_L)}+\frac{S_2\left(\rho^2-\rho_N^2\right)}{6E_2^1(\rho)E_2^1(\rho_N)}\right]\frac{\mathbb{E}_2^1(\boldsymbol{r})}{\Lambda-\Lambda'}\\ &+\left[(S_1-S_2)\frac{V(\rho_N)}{4\pi}I_2^2(\rho_N,\rho_L)+\frac{S_1\left(\rho_N^2-\rho_L^2\right)}{6E_2^2(\rho_N)E_2^2(\rho_L)}+\frac{S_2\left(\rho^2-\rho_N^2\right)}{6E_2^2(\rho)E_2^2(\rho_N)}\right]\frac{\mathbb{E}_2^2(\boldsymbol{r})}{\Lambda-\Lambda'}\end{aligned} \tag{3.19}$$

and the pressure distribution in the living shell:

$$\begin{aligned}\bar{p}_L=&\left[\bar{g}(\rho_L)+(S_1-S_2)\frac{V(\rho_N)}{4\pi}I_0^1(\rho,\rho_L)+\frac{S_1}{6}\left(\rho^2-\rho_L^2\right)\right]\\ &-\left[(S_1-S_2)\frac{V(\rho_N)}{4\pi}I_2^1(\rho,\rho_L)+\frac{S_1}{6}\frac{\rho^2-\rho_L^2}{E_2^1(\rho)E_2^1(\rho_L)}\right]\frac{\mathbb{E}_2^1(\boldsymbol{r})}{\Lambda-\Lambda'}\\ &+\left[(S_1-S_2)\frac{V(\rho_N)}{4\pi}I_2^2(\rho,\rho_L)+\frac{S_1}{6}\frac{\rho^2-\rho_L^2}{E_2^2(\rho)E_2^2(\rho_L)}\right]\frac{\mathbb{E}_2^2(\boldsymbol{r})}{\Lambda-\Lambda'}\ .\end{aligned} \tag{3.20}$$

Lastly, we introduce the following equation for the evolution of the unperturbed ellipsoidal outer boundary of the tumour:

$$\frac{\mathrm{d}\rho_L}{\mathrm{dt}} = -\left[S_1\frac{V(\rho_L)-V(\rho_N)}{V(\rho_L)} + S_2\frac{V(\rho_N)}{V(\rho_L)}\right]\frac{\rho_L\left(\rho_L^2-\mu^2\right)\left(\rho_L^2-\nu^2\right)}{3E_2^1(\rho_L)E_2^2(\rho_L)} + \frac{\beta}{d_t}\left(\rho_L-\rho_Q\right) \ . \quad (3.21)$$

Using the parameters in Table 1 below we plot equation (3.21) in time, and the result is depicted in Figure 2. It shows that the unperturbed boundary soon reaches the steady

TABLE 1. Parameters for plotting the graphs

Parameters	Values
α_1	7.2/1000
α_2	5/1000
α_3	6/1000
S_1	4
S_2	1000
σ_1	0.9
σ_2	0.4
σ_∞	1
γ/k	1
β/d_t	4
$\rho_L(t=0)$	16/1000

state value, 24.41/1000, from the initial value of 16/1000.

4. Perturbed part. For the perturbed part of the tumour we focus on the variables with the tilde on the top ($\tilde{\sigma}_N$, $\tilde{\sigma}_L$, $\tilde{\sigma}_S$, $\tilde{p}_N$, $\tilde{p}_L$, $\tilde{p}_S$) and the evolution of the perturbation, f, which is assumed to depend only on μ, ν and on time, t. The perturbed nutrient concentration is governed by the Laplace equation

$$\Delta\tilde{\sigma}_N = 0 \ , \quad (4.1)$$

$$\Delta\tilde{\sigma}_L = 0 \ , \quad (4.2)$$

$$\Delta\tilde{\sigma}_S = 0 \quad (4.3)$$

in the necrotic core, the living shell and the surrounding area of the tumour, respectively. The perturbed pressure distribution within the tumour could no longer be obtained by solving the Poisson equation, but simply by the following Laplace equations:

$$\Delta\tilde{p}_N = 0 \ , \quad (4.4)$$

$$\Delta\tilde{p}_L = 0 \ , \quad (4.5)$$

where $\tilde{p}_N$ is the perturbed pressure in the necrotic core and $\tilde{p}_L$ the perturbed pressure in the living layer. The equations of continuity on the interface between the necrotic part

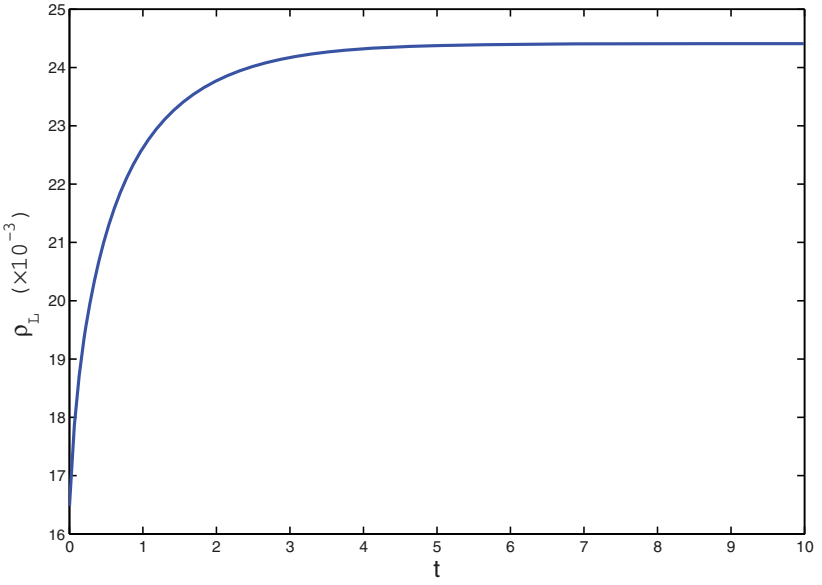

FIG. 2. Boundary evolution of the unperturbed part versus time

and the living part of the tumour, i.e. equations (2.12)-(2.14), are transformed into the following equations:

$$\tilde{\sigma}_N = \tilde{\sigma}_L \ , \tag{4.6}$$

$$\tilde{p}_N = \tilde{p}_L \ , \tag{4.7}$$

$$\frac{\partial \tilde{p}_N}{\partial \rho} = \frac{\partial \tilde{p}_L}{\partial \rho} \tag{4.8}$$

after we introduce equations (2.22)-(2.26) and the expression for the normal unit vector on the interface, which can be found in Appendix B. The boundary conditions on the outer boundary of the tumour are turned into more complicated expressions, due to the fact that the boundary (ρ_L), the curvature (κ), the normal unit vector ($\hat{\boldsymbol{n}}$) and the gradient on the outer boundary of the tumour are all expressed in terms of ε. The expressions for $\hat{\boldsymbol{n}}$ are ∇ can be found in Appendix B. Finally, equation (2.15) assumes the form

$$\begin{aligned}\frac{\partial \tilde{\sigma}_L}{\partial \rho} + \left(-\frac{f\rho_L}{\rho_L^2-\mu^2} - \frac{f\rho_L}{\rho_L^2-\nu^2} + \frac{f\rho_L}{\rho_L^2-h_3^2} + \frac{f\rho_L}{\rho_L^2-h_2^2} \right) \left[\frac{\partial \bar{\sigma}_L}{\rho} + \frac{\gamma}{k} \left(h_\rho^L\right)^2 (\rho_L - \rho_Q) \right] \\ = \frac{\left(h_\rho^L\right)^2}{\left(h_\nu^L h_\mu^L\right)^2} \left\{ \frac{(h_\mu^L)^2}{\rho_L^2-\nu^2} \frac{\partial \bar{\sigma}_L}{\partial \nu} \left[f_\nu \sqrt{\rho_L^2-\nu^2} - \frac{\nu f}{\sqrt{\rho_L^2-\nu^2}} \right] \right. \\ \left. + \frac{(h_\nu^L)^2}{\rho_L^2-\mu^2} \frac{\partial \bar{\sigma}_L}{\partial \mu} \frac{\partial}{\partial \mu} \left[f_\mu \sqrt{\rho_L^2-\mu^2} - \frac{\mu f}{\sqrt{\rho_L^2-\mu^2}} \right] \right\} + \frac{\gamma}{k} f \ , \end{aligned} \tag{4.9}$$

while equation (2.16) retains its simple form:

$$\tilde{\sigma}_L = \tilde{\sigma}_S \ . \tag{4.10}$$

The metric coefficients on the outer boundary are also expressed in terms of ε (Appendix B). Equation (2.17) for the perturbed part has the form

$$\left(h_\rho^L\right)^2 f_t + \frac{\partial \tilde{p}_L}{\partial \rho} - \frac{\beta}{d_t}\left(h_\rho^L\right)^2 f + f\rho_L\left(\frac{1}{\rho_L^2-\mu^2}+\frac{1}{\rho_L^2-\nu^2}-\frac{1}{\rho_L^2-h_3^2}-\frac{1}{\rho_L^2-h_2^2}\right)$$
$$\cdot\left[\left(h_\rho^L\right)^2\frac{\mathrm{d}\rho_L}{\mathrm{dt}} - \frac{\partial \bar{p}_L}{\partial \rho} - \frac{\beta}{d_t}\left(h_\rho^L\right)^2(\rho_L-\rho_Q)\right] + \left(\frac{\mu f}{\rho_L^2-\mu^2}-f_\mu\right)\left(h_\rho^L\right)^2\left[\frac{\mathrm{d}\mu}{\mathrm{dt}}+\frac{1}{\left(h_\mu^L\right)^2}\frac{\partial \bar{p}_L}{\partial \mu}\right]$$
$$+\left(\frac{\nu f}{\rho_L^2-\nu^2}-f_\nu\right)\left(h_\rho^L\right)^2\left[\frac{\mathrm{d}\nu}{\mathrm{dt}}+\frac{1}{\left(h_\nu^L\right)^2}\frac{\partial \bar{p}_L}{\partial \nu}\right]=0\ , \quad (4.11)$$

while equation (2.18) splits into three different equations:

$$\left(f_\nu-\frac{\nu f}{\rho_L^2-\nu^2}\right)\left[\left(h_\mu^L\right)^2\frac{\mathrm{d}\mu}{\mathrm{dt}}-\frac{\partial \bar{p}_L}{\partial \mu}\right]=\left(f_\mu-\frac{\mu f}{\rho_L^2-\mu^2}\right)\left[\left(h_\nu^L\right)^2\frac{\mathrm{d}\nu}{\mathrm{dt}}-\frac{\partial \bar{p}_L}{\partial \nu}\right]\ , \quad (4.12)$$

$$\frac{\partial \tilde{p}_L}{\partial \mu}=\left(f_\mu-\frac{\mu f}{\rho_L^2-\mu^2}\right)\left[\left(h_\rho^L\right)^2\frac{\mathrm{d}\rho_L}{\mathrm{dt}}-\frac{\partial \bar{p}_L}{\partial \rho}\right]+\frac{f\rho_L}{\rho_L^2-\mu^2}\left[\left(h_\mu^L\right)^2\frac{\mathrm{d}\mu}{\mathrm{d}t}+\frac{\partial \bar{p}_L}{\partial \mu}\right]\ , \quad (4.13)$$

$$\frac{\partial \tilde{p}_L}{\partial \nu}=\left(f_\nu-\frac{\nu f}{\rho_L^2-\nu^2}\right)\left[\left(h_\rho^L\right)^2\frac{\mathrm{d}\rho_L}{\mathrm{dt}}-\frac{\partial \bar{p}_L}{\partial \rho}\right]+\frac{f\rho_L}{\rho_L^2-\nu^2}\left[\left(h_\nu^L\right)^2\frac{\mathrm{d}\nu}{\mathrm{d}t}+\frac{\partial \bar{p}_L}{\partial \nu}\right]\ . \quad (4.14)$$

Next, the pressure from inside the tumour reaches a constant value on the boundary, $\tilde{g}(\rho_L)$. Depending on the boundary we obtain

$$\tilde{p}_L=\tilde{g}(\rho_L)\ , \quad (4.15)$$

$$\tilde{p}_S=\tilde{g}(\rho_L)-\alpha\tilde{\kappa}\ , \quad (4.16)$$

because of our assumption of the Young-Laplace equation (2.19). For the perturbed nutrient concentration near the nutrient source we assume

$$\tilde{\sigma}_S\to 0,\ \text{as}\ |\boldsymbol{r}|\to\infty\ . \quad (4.17)$$

We consider harmonic solutions for the perturbation, the nutrient concentration and the pressure distribution:

$$f = \sum_{n=0}^{\infty}\sum_{m=1}^{2n+1} a_n^m(t)E_n^m(\rho)S_n^m(\mu,\nu) \ , \tag{4.18}$$

$$\tilde{\sigma}_N = \sum_{n=0}^{\infty}\sum_{m=1}^{2n+1} b_n^m(t)E_n^m(\rho)S_n^m(\mu,\nu) \ , \tag{4.19}$$

$$\tilde{\sigma}_L = \sum_{n=0}^{\infty}\sum_{m=1}^{2n+1} \left[c_n^m(t) + (2n+1)\, d_n^m(t)I_n^m(\rho)\right] E_n^m(\rho)S_n^m(\mu,\nu) \ , \tag{4.20}$$

$$\tilde{p}_N = \sum_{n=0}^{\infty}\sum_{m=1}^{2n+1} e_n^m(t)E_n^m(\rho)S_n^m(\mu,\nu) \ , \tag{4.21}$$

$$\tilde{p}_L = \sum_{n=0}^{\infty}\sum_{m=1}^{2n+1} \left[g_n^m(t) + (2n+1)\, h_n^m(t)I_n^m(\rho)\right] E_n^m(\rho)S_n^m(\mu,\nu) \ , \tag{4.22}$$

$$\tilde{\sigma}_S = \sum_{n=0}^{\infty}\sum_{m=1}^{2n+1} (2n+1)\, i_n^m(t)I_n^M(\rho)E_n^m(\rho)S_n^m(\mu,\nu) \ , \tag{4.23}$$

where $a_n^m(t)$, $b_n^m(t)$, $c_n^m(t)$, $d_n^m(t)$, $e_n^m(t)$, $g_n^m(t)$, $h_n^m(t)$, $i_n^m(t)$ are time-dependent coefficients, $E_n^m(\rho)$ are the Lamé functions of the first kind, $S_n^m(\mu,\nu)$ the ellipsoidal surface harmonics and $I_n^m(\rho)$ the elliptic integrals. $E_n^m(\rho)$, $S_n^m(\mu,\nu)$, $I_n^m(\rho)$ are defined in Appendix A.

In order to determine whether the tumour is stable or not, we need to know whether f increases or decays. To do that, we need the following equation:

$$\begin{aligned}
\left(h_\rho^L\right)^2 \sum_{n=0}^{\infty}\sum_{m=1}^{2n+1} a_n^{m'}(t)E_n^m(\rho)S_n^m(\mu,\nu) + \sum_{n=0}^{\infty}\sum_{m=1}^{2n+1} g_n^m(t)\frac{\partial E_n^m(\rho)}{\partial\rho}S_n^m(\mu,\nu) \\
- \frac{\beta}{d_t}\left(h_\rho^L\right)^2 \sum_{n=0}^{\infty}\sum_{m=1}^{2n+1} a_n^m(t)E_n^m(\rho)S_n^m(\mu,\nu) \\
- \frac{2}{3}\rho_L^2\left[\sum_{n=0}^{\infty}\sum_{m=1}^{2n+1} a_n^m(t)E_n^m(\rho)S_n^m(\mu,\nu)\right]\left(\frac{1}{\rho_L^2-\mu^2}+\frac{1}{\rho_L^2-\nu^2}-\frac{1}{\rho_L^2-h_3^2}-\frac{1}{\rho_L^2-h_2^2}\right) \\
\cdot\left[S_1\frac{V(\rho_L)-V(\rho_N)}{V(\rho_L)}+S_2\frac{V(\rho_N)}{V(\rho_L)}\right]\frac{\left(\rho_L^2-\mu^2\right)\left(\rho_L^2-\nu^2\right)}{E_2^1(\rho_L)E_2^2(\rho_L)} = 0 \ ,
\end{aligned} \tag{4.24}$$

which includes the time-derivative of the coefficient of the perturbation, $a_n^{m'}(t)$. However, there is also the coefficient of $\tilde{p}_L$. So, in need of a second equation between $g_n^m(t)$ and

$a_n^m(t)$ we choose the following equation:

$$\sum_{n=0}^{\infty}\sum_{m=1}^{2n+1} g_n^m(t)E_n^m(\rho_L)\frac{\partial E_n^m(\mu)}{\partial \mu}E_n^m(n)$$
$$= \frac{\left(h_\rho^L\right)^2}{\sqrt{\rho_L^2-\nu^2}}\frac{\partial}{\partial \mu}\left[\sqrt{\rho_L^2-\mu^2}\sum_{n=0}^{\infty}\sum_{m=1}^{2n+1} a_n^m(t)\mathbb{E}_n^m(\boldsymbol{r}_L)\right]$$
$$\cdot\left\{-\frac{2\rho_L}{3\left(h_\rho^L\right)^2}\left[S_1-(S_1-S_2)\frac{V(\rho_N)}{V(\rho_L)}\right]\frac{\left(\rho_L^2-\mu^2\right)\left(\rho_L^2-\nu^2\right)}{E_2^1(\rho_L)E_2^2(\rho_L)}+\frac{\beta}{d_t}\left(\rho_L-\rho_Q\right)\right\}. \quad (4.25)$$

In Figures (3)-(5), we depict the ratio $\frac{a_n^{m'}}{a_n^m}$ by combining equations (4.24) and (4.25) in the $\mu-\nu$ contour. In order to conclude whether f increases, the above fraction must be positive. When the fraction is negative, then f decays. As seen in the following figures, using the parameters from Table 1, f increases in all cases.

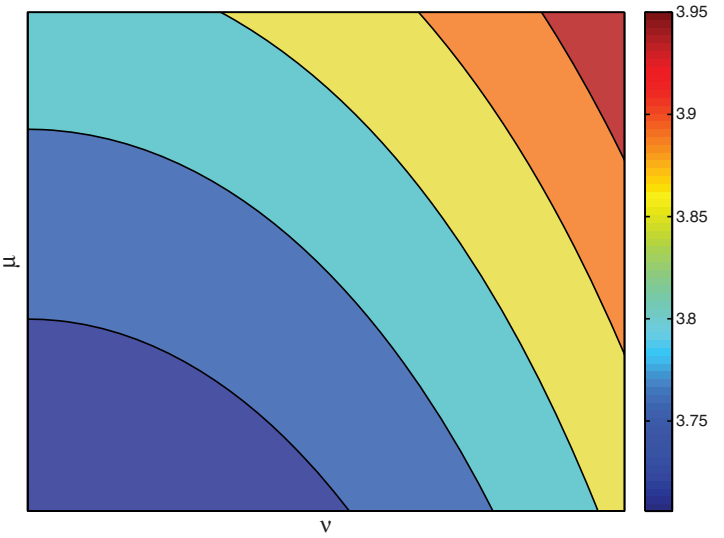

FIG. 3. The μ,ν contour for $n=0$ and $m=0$

This contradicts the spherical case, as predicted by Greenspan, where there were different cases of f being amplified or decayed depending on the tumour unperturbed radius. However, in the ellipsoidal case, the anisotropy of the shape inclines towards the legitimacy of this result. In other words, in a system less symmetrical than the sphere, we expect the asymmetry to reflect unstable tumour growth from the very start of its development.

It is depressing to realize that most tumours do not develop in a symmetric way and therefore no stability of their growth is expected. This is another physical case where instability appears as a result of lack of symmetry.

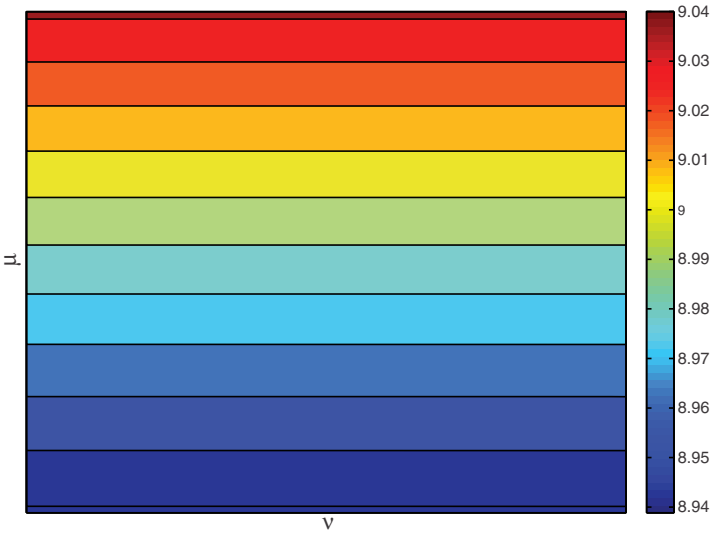

FIG. 4. The μ, ν contour for $n = 1$ and $m = 1$

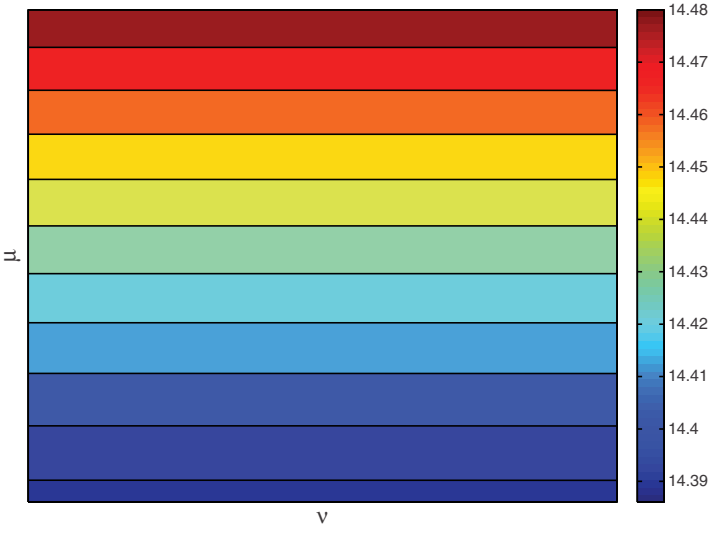

FIG. 5. The μ, ν contour for $n = 2$ and $m = 1$

5. Appendices.

A. The ellipsoidal system. The anisotropy of the ellipsoidal coordinate system serves as a better tool to approach shapes more complicated than simple spheres. The reference ellipsoid is specified when given any three numbers $\alpha_1,\ \alpha_2,\ \alpha_3$ via the equation

$$\frac{x_1^2}{\alpha_1^2}+\frac{x_2^2}{\alpha_2^2}+\frac{x_3^2}{\alpha_3^2}=1,\ 0<\alpha_2<\alpha_2<\alpha_1<+\infty, \tag{A.1}$$

where $\alpha_1,\ \alpha_2,\ \alpha_3$ are the three semi–axes of the ellipsoid which in turn define the semi–focal distances

$$h_1^2=\alpha_2^2-\alpha_3^2,\ h_2^2=\alpha_1^2-\alpha_3^2,\ h_3^2=\alpha_1^2-\alpha_2^2. \tag{A.2}$$

The core of the ellipsoidal coordinate system is the focal ellipse, an ellipse on the x_1, x_2 plane with semi–focal distance h_3 and semi–axes h_1 and h_2.

As depicted in Figure 6 the variable ρ defines a family of confocal ellipsoids, the variable μ defines a confocal family of hyperboloids of one sheet, while the variable ν defines a confocal family of hyperboloids of two sheets. The ellipsoidal coordinates are

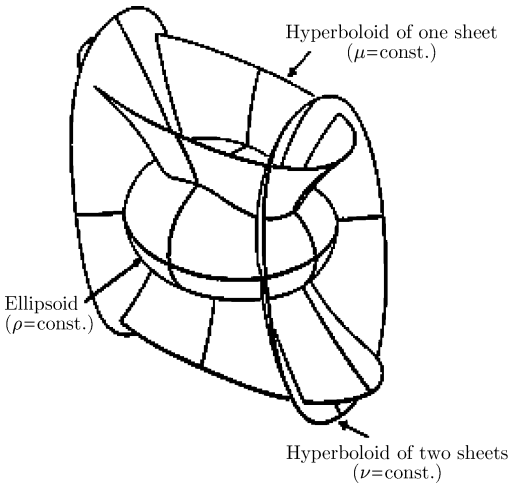

FIG. 6. Ellipsoidal Coordinate System

connected with the coordinates of the Cartesian system as

$$x_1 = \frac{\rho\mu\nu}{h_2h_3},\ h_2<\rho<+\infty, \tag{A.3}$$

$$x_2 = \frac{\sqrt{\rho^2-h_3^2}\sqrt{\mu^2-h_3^2}\sqrt{h_3^2-\nu^2}}{h_1h_3},\ h_3<\mu<h_2, \tag{A.4}$$

$$x_3 = \frac{\sqrt{\rho^2-h_2}\sqrt{h_2^2-\mu^2}\sqrt{h_2^2-\nu^2}}{h_1h_2}, 0<\nu<h_3. \tag{A.5}$$

The ellipsoidal metric coefficients are given by

$$h_\rho = ||\boldsymbol{r}_\rho|| = \frac{\sqrt{\rho^2-\mu^2}\sqrt{\rho^2-\nu^2}}{\sqrt{\rho^2-h_3^2}\sqrt{\rho^2-h_2^2}}, \tag{A.6}$$

$$h_\mu = ||\boldsymbol{r}_\mu|| = \frac{\sqrt{\rho^2-\mu^2}\sqrt{\mu^2-\nu^2}}{\sqrt{\mu^2-h_3}\sqrt{h_2^2-\mu^2}}, \tag{A.7}$$

$$h_\nu = ||\boldsymbol{r}_\nu|| = \frac{\sqrt{\rho^2-\nu^2}\sqrt{\mu^2-\nu^2}}{\sqrt{h_3^2-\nu^2}\sqrt{h_2^2-\nu^2}}. \tag{A.8}$$

The relative solutions to the Laplace equation differ depending on the domain wherein they are defined. An interior harmonic solution has the form of

$$\mathbb{E}_n^m(\rho,\mu,\nu) = E_n^m(\rho)E_n^m(\mu)E_n^m(\nu), \tag{A.9}$$

where E_n^m is the Lamé function of the first kind, of degree $n = 0, 1, 2, \ldots$ and order $m = 1, 2, \ldots 2n+1$, whereas an exterior harmonic solution is defined as

$$\mathbb{F}_n^m(\rho,\mu,\nu) = F_n^m(\rho)E_n^m(\mu)E_n^m(\nu), \tag{A.10}$$

where F_n^m is the Lamé function of the second kind. The latter is given by

$$F_n^m(\rho) = (2n+1)E_n^m(\rho)\int_\rho^\infty \frac{\mathrm{d}x}{[E_n^m(x)]^2\sqrt{x^2-h_3^2}\sqrt{x^2-h_2^2}}. \tag{A.11}$$

The functions $\mathbb{E}_n^m(\rho,\mu,\nu)$ and $\mathbb{F}_n^m(\rho,\mu,\nu)$ are called Lamé products or interior and exterior ellipsoidal harmonics, respectively. The surface ellipsoidal harmonics are given by

$$S_n^m(\mu,\nu) = E_n^m(\mu)E_n^m(\nu),\ n = 0, 1, 2, \ldots, m = 1, 2, \ldots, 2n+1. \tag{A.12}$$

Lastly, we will state the ellipsoidal harmonics of degree less than or equal to two because these are the harmonics used in this work. For $n = 0$, we have the Lamé function

$$E_0^1(x) = 1, \tag{A.13}$$

where x is one of the ellipsoidal coordinates $(\rho,\ \mu,\ \nu)$, the interior ellipsoidal harmonic

$$\mathbb{E}_0^1(\rho,\mu,\nu) = 1, \tag{A.14}$$

and the exterior ellipsoidal harmonic

$$\mathbb{F}_0^1(\rho,\mu,\nu) = \int_\rho^\infty \frac{\mathrm{d}x}{\sqrt{x^2-h_3^2}\sqrt{x^2-h_2^2}}. \tag{A.15}$$

For $n = 1$, we have the Lamé functions

$$E_1^1(x) = x, \tag{A.16}$$

$$E_1^2(x) = \sqrt{|x^2-h_3^2|}, \tag{A.17}$$

$$E_1^3(x) = \sqrt{|x^2-h_2^2|}, \tag{A.18}$$

the interior ellipsoidal harmonics:

$$\mathbb{E}_1^1(\rho,\mu,\nu) = \rho\mu\nu = h_2h_3x_1, \tag{A.19}$$

$$\mathbb{E}_1^2(\rho,\mu,\nu) = \sqrt{\rho^2-h_3^2}\sqrt{\mu^2-h_3^2}\sqrt{h_3^2-\nu^2} = h_1h_3x_2, \tag{A.20}$$

$$\mathbb{E}_1^3(\rho,\mu,\nu) = \sqrt{\rho^2-h_2^2}\sqrt{h_2^2-\mu^2}\sqrt{h_2^2-\nu^2} = h_1h_2x_3, \tag{A.21}$$

and the exterior ellipsoidal harmonics:

$$\mathbb{F}_1^1(\rho,\mu,\nu) = 3\mathbb{E}_1^1(\rho,\mu,\nu)\int_\rho^\infty \frac{\mathrm{d}x}{x^2\sqrt{x^2-h_3^2}\sqrt{x_2^2-h_2^2}}, \tag{A.22}$$

$$\mathbb{F}_1^2(\rho,\mu,\nu) = 3\mathbb{E}_1^2(\rho,\mu,\nu)\int_\rho^\infty \frac{\mathrm{d}x}{(x^2-h_3^2)^{3/2}\sqrt{x_2^2-h_2^2}}, \tag{A.23}$$

$$\mathbb{F}_1^3(\rho,\mu,\nu) = 3\mathbb{E}_1^3(\rho,\mu,\nu)\int_\rho^\infty \frac{\mathrm{d}x}{\sqrt{x^2-h_3^2}(x_2^2-h_2^2)^{3/2}}. \tag{A.24}$$

For $n=2$, we have the Lamé functions

$$E_2^1(x) = x^2+\Lambda-\alpha_1^2, \tag{A.25}$$

$$E_2^2(x) = x^2+\Lambda'-\alpha_1^2, \tag{A.26}$$

$$E_2^3(x) = x\sqrt{|x^2-h_3^2|}, \tag{A.27}$$

$$E_2^4(x) = x\sqrt{|x^2-h_2^2|}, \tag{A.28}$$

$$E_2^5(x) = \sqrt{|x^2-h_3^2|}\sqrt{|x^2-h_2^2|}, \tag{A.29}$$

where

$$\Lambda = \frac{1}{3}\left(a_1^2+a_2^2+a_3^2\right)+\frac{1}{3}\sqrt{h_1^4+h_2^2h_3^2}, \tag{A.30}$$

$$\Lambda' = \frac{1}{3}\left(a_1^2+a_2^2+a_3^2\right)-\frac{1}{3}\sqrt{h_1^4+h_2^2h_3^2}. \tag{A.31}$$

The interior ellipsoidal harmonics for $n=2$ are

$$\mathbb{E}_2^1(\rho,\mu,\nu) = (\rho^2+\Lambda-\alpha_1^2)(\mu^2+\Lambda-\alpha_1^2)(\nu^2+\Lambda-\alpha_1^2), \tag{A.32}$$

$$\mathbb{E}_2^2(\rho,\mu,\nu) = (\rho^2+\Lambda'-\alpha_1^2)(\mu^2+\Lambda'-\alpha_1^2)(\nu^2+\Lambda'-\alpha_1^2), \tag{A.33}$$

$$\mathbb{E}_2^3(\rho,\mu,\nu) = \rho\mu\nu\sqrt{\rho^2-h_3^2}\sqrt{\mu^2-h_3^2}\sqrt{h_3^2-\nu^2}, \tag{A.34}$$

$$\mathbb{E}_2^4(\rho,\mu,\nu) = \rho\mu\nu\sqrt{\rho^2-h_2^2}\sqrt{h_2^2-\mu^2}\sqrt{h_2^2-\nu^2}, \tag{A.35}$$

$$\mathbb{E}_2^5(\rho,\mu,\nu) = \sqrt{\rho^2-h_3^2}\sqrt{\mu^2-h_3^2}\sqrt{h_3^2-\nu^2}\sqrt{\rho^2-h_2^2}\sqrt{h_2^2-\mu^2}\sqrt{h_2^2-\nu^2}, \tag{A.36}$$

and the exterior ellipsoidal harmonics are given by

$$\mathbb{F}_2^1(\rho,\mu,\nu) = 5\mathbb{E}_2^1(\rho,\mu,\nu)\int_\rho^\infty \frac{\mathrm{d}x}{\left(x^2+\Lambda-\alpha_1^2\right)^2\sqrt{x^2-h_3^2}\sqrt{x_2^2-h_2^2}}, \tag{A.37}$$

$$\mathbb{F}_2^2(\rho,\mu,\nu) = 5\mathbb{E}_2^2(\rho,\mu,\nu)\int_\rho^\infty \frac{\mathrm{d}x}{\left(x^2+\Lambda'-\alpha_1^2\right)^2\sqrt{x^2-h_3^2}\sqrt{x_2^2-h_2^2}}, \tag{A.38}$$

$$\mathbb{F}_2^3(\rho,\mu,\nu) = 5\mathbb{E}_2^3(\rho,\mu,\nu)\int_\rho^\infty \frac{\mathrm{d}x}{x^2\left(x^2-h_3^2\right)^{3/2}\sqrt{x_2^2-h_2^2}}, \tag{A.39}$$

$$\mathbb{F}_2^4(\rho,\mu,\nu) = 5\mathbb{E}_2^4(\rho,\mu,\nu)\int_\rho^\infty \frac{\mathrm{d}x}{x^2\left(x^2-h_2^2\right)^{3/2}\sqrt{x^2-h_3^2}}, \tag{A.40}$$

$$\mathbb{F}_2^5(\rho,\mu,\nu) = 5\mathbb{E}_2^5(\rho,\mu,\nu)\int_\rho^\infty \frac{\mathrm{d}x}{\left(x^2-h_3^2\right)^{3/2}\left(x^2-h_2^2\right)^{3/2}}. \tag{A.41}$$

B. Useful expressions. In this appendix, we will present the expressions for the metric coefficients, the normal unit vectors and the gradient for all areas and boundaries of the tumour. We begin with the metric coefficients of the boundary of the necrotic core:

$$h_\rho^N = \frac{\sqrt{\rho_N^2-\mu^2}\sqrt{\rho_N^2-\nu^2}}{\sqrt{\rho_N^2-h_3^2}\sqrt{\rho_N^2-h_2^2}}, \tag{B.1}$$

$$h_\mu^N = \frac{\sqrt{\rho_N^2-\mu^2}\sqrt{\mu^2-\nu^2}}{\sqrt{\mu^2-h_3^2}\sqrt{h_2^2-\mu^2}}, \tag{B.2}$$

$$h_\nu^N = \frac{\sqrt{\rho_N^2-\nu^2}\sqrt{\mu^2-\nu^2}}{\sqrt{h_3^2-\nu^2}\sqrt{h_2^2-\nu^2}}. \tag{B.3}$$

Then, we state the metric coefficients for the boundary of the unperturbed ellipsoidal tumour:

$$h_\rho^L = \frac{\sqrt{\rho_L^2-\mu^2}\sqrt{\rho_L^2-\nu^2}}{\sqrt{\rho_P^2-h_3^2}\sqrt{\rho_L^2-h_2^2}}, \tag{B.4}$$

$$h_\mu^L = \frac{\sqrt{\rho_L^2-\mu^2}\sqrt{\mu^2-\nu^2}}{\sqrt{\mu^2-h_3^2}\sqrt{h_2^2-\mu^2}}, \tag{B.5}$$

$$h_\nu^L = \frac{\sqrt{\rho_L^2-\nu^2}\sqrt{\mu^2-\nu^2}}{\sqrt{h_3^2-\nu^2}\sqrt{h_2^2-\nu^2}}. \tag{B.6}$$

However, on the tumour surface, the metric coefficients are expressed in terms of the perturbation parameter ε:

$$h_\rho = \frac{\sqrt{\rho^2-\mu^2}\sqrt{\rho^2-\nu^2}}{\sqrt{\rho^2-h_3^2}\sqrt{\rho^2-h_2^2}} \Rightarrow h_\rho = \frac{\sqrt{\left(\rho_L+\varepsilon f\right)^2-\mu^2}\sqrt{\left(\rho_L+\varepsilon f\right)^2-\nu^2}}{\sqrt{\left(\rho_L+\varepsilon f\right)^2-h_3^2}\sqrt{\left(\rho_L+\varepsilon f\right)^2-h_2^2}}$$
$$\Rightarrow h_\rho = h_\rho^L\left[1+\frac{\varepsilon\rho_L f}{\rho_L^2-\mu^2}+\frac{\varepsilon\rho_L f}{\rho_L^2-\nu^2}-\frac{\varepsilon\rho_L f}{\rho_L^2-h_3^2}-\frac{\varepsilon\rho_L f}{\rho_L^2-h_2^2}+\mathcal{O}\left(\varepsilon^2\right)\right], \tag{B.7}$$

$$h_\mu = \frac{\sqrt{\rho^2-\mu^2}\sqrt{\mu^2-\nu^2}}{\sqrt{\mu^2-h_3^2}\sqrt{h_2^2-\mu^2}} \Rightarrow h_\mu = \frac{\sqrt{\left(\rho_L+\varepsilon f\right)^2-\mu^2}\sqrt{\mu^2-\nu^2}}{\sqrt{\mu^2-h_3^2}\sqrt{h_2^2-\mu^2}}$$
$$\Rightarrow h_\mu = h_\mu^L\left[1+\frac{\varepsilon\rho_L f}{\rho_L^2-\mu^2}+\mathcal{O}\left(\varepsilon^2\right)\right], \quad \text{(B.8)}$$

$$h_\nu = \frac{\sqrt{\rho^2-\nu^2}\sqrt{\mu^2-\nu^2}}{\sqrt{h_3^2-\nu^2}\sqrt{h_2^2-\nu^2}} \Rightarrow h_\nu = \frac{\sqrt{\left(\rho_L+\varepsilon f\right)^2-\nu^2}\sqrt{\mu^2-\nu^2}}{\sqrt{h_3^2-\nu^2}\sqrt{h_2^2-\nu^2}}$$
$$\Rightarrow h_\nu = h_\nu^L\left[1+\frac{\varepsilon\rho_L f}{\rho_L^2-\nu^2}+\mathcal{O}\left(\varepsilon^2\right)\right]. \quad \text{(B.9)}$$

For this model, we will need the reciprocals of the metric coefficients, which are

$$\frac{1}{h_\rho} = \frac{1}{h_\rho^L}\left[1-\frac{\varepsilon\rho_L f}{\rho_L^2-\mu^2}-\frac{\varepsilon\rho_L f}{\rho_L^2-\nu^2}+\frac{\varepsilon\rho_L f}{\rho_L^2-h_3^2}+\frac{\varepsilon\rho_L f}{\rho_L^2-h_2^2}+\mathcal{O}\left(\varepsilon^2\right)\right], \quad \text{(B.10)}$$

$$\frac{1}{h_\mu} = \frac{1}{h_\mu^L}\left[1-\frac{\varepsilon\rho_L f}{\rho_L^2-\mu^2}+\mathcal{O}\left(\varepsilon^2\right)\right], \quad \text{(B.11)}$$

$$\frac{1}{h_\nu} = \frac{1}{h_\nu^L}\left[1-\frac{\varepsilon\rho_L f}{\rho_L^2-\nu^2}+\mathcal{O}\left(\varepsilon^2\right)\right]. \quad \text{(B.12)}$$

The boundary of the necrotic core retains its original ellipsoidal shape. This boundary is changing only on the ρ direction of the ellipsoidal coordinate system. So, the normal unit vector is obtained by

$$\hat{\boldsymbol{n}} = \hat{\boldsymbol{\rho}}_0, \quad \text{(B.13)}$$

while the expression for the gradient on $\partial\Omega_N$ has the form

$$\nabla = \frac{\hat{\boldsymbol{\rho}}_0}{h_\rho^N}\frac{\partial}{\partial\rho}+\frac{\hat{\boldsymbol{\mu}}_0}{h_\mu^N}\frac{\partial}{\partial\mu}+\frac{\hat{\boldsymbol{\nu}}_0}{h_\nu^N}\frac{\partial}{\partial\nu}. \quad \text{(B.14)}$$

For $\partial\Omega_P$, the normal unit vector is expressed in terms of ε as

$$\hat{\boldsymbol{n}} = \hat{\boldsymbol{\rho}}_0+\varepsilon h_\rho^L f\left[\frac{\nu\hat{\boldsymbol{\nu}}_0}{h_\nu^P\left(\rho_L^2-\nu^2\right)}+\frac{\mu\hat{\boldsymbol{\mu}}_0}{h_\mu^P\left(\rho_L^2-\mu^2\right)}\right]-\varepsilon\frac{h_\rho^L}{h_\nu^L}f_\nu\hat{\boldsymbol{\nu}}_0-\varepsilon\frac{h_\rho^L}{h_\mu^L}f_\mu\hat{\boldsymbol{\mu}}_0+\mathcal{O}\left(\varepsilon^2\right), \quad \text{(B.15)}$$

and the gradient on the outer boundary has the form

$$\nabla = \frac{\hat{\boldsymbol{\rho}}_0}{h_\rho}\frac{\partial}{\partial\rho}+\frac{\hat{\boldsymbol{\mu}}_0}{h_\mu}\frac{\partial}{\partial\mu}+\frac{\hat{\boldsymbol{\nu}}_0}{h_\nu}\frac{\partial}{\partial\nu}-\varepsilon f\rho_L\frac{\hat{\boldsymbol{\rho}}_0}{h_\rho^L}\left(\frac{1}{\rho_L^2-\mu^2}+\frac{1}{\rho_L^2-\nu^2}-\frac{1}{\rho_L^2-h_3^2}-\frac{1}{\rho_L^2-h_2^2}\right)\frac{\partial}{\partial\rho}$$
$$-\varepsilon f\rho_L\left[\frac{\hat{\boldsymbol{\mu}}_0}{h_\mu^L}\frac{1}{\rho_L^2-\mu^2}\frac{\partial}{\partial\mu}+\frac{\hat{\boldsymbol{\nu}}_0}{h_\nu^L}\frac{1}{\rho_L^2-\nu^2}\frac{\partial}{\partial\nu}\right]+\mathcal{O}\left(\varepsilon^2\right). \quad \text{(B.16)}$$

For this approach we will also need an expression for the evolution of the outer boundary in terms of ε, which is

$$\frac{\mathrm{d}\rho_L}{\mathrm{dt}} = h_\rho^L\left\{\frac{\mathrm{d}\rho_L}{\mathrm{dt}}+\varepsilon\left[f_t+f\rho_L\left(\frac{1}{\rho_L^2-\mu^2}+\frac{1}{\rho_L^2-\nu^2}-\frac{1}{\rho_L^2-h_3^2}-\frac{1}{\rho_L^2-h_2^2}\right)\frac{\mathrm{d}\rho_L}{\mathrm{dt}}\right]\right\}\hat{\boldsymbol{\rho}}_0$$
$$+h_\mu^L\left(1+\frac{\varepsilon f\rho_L}{\rho_L^2-\mu^2}\right)\frac{\mathrm{d}\mu}{\mathrm{dt}}\hat{\boldsymbol{\mu}}_0+h_\nu^L\left(1+\frac{\varepsilon f\rho_L}{\rho_L^2-\nu^2}\right)\frac{\mathrm{d}\nu}{\mathrm{dt}}\hat{\boldsymbol{\nu}}_0+\mathcal{O}\left(\varepsilon^2\right). \quad \text{(B.17)}$$

Most of the above formulae were taken from the paper by [20] and the relative book ([19]).

References

[1] T. Alarcón, H. M. Byrne, and P. K. Maini, *A multiple scale model for tumor growth*, Multiscale Model. Simul. **3** (2005), no. 2, 440–475, DOI 10.1137/040603760. MR2122996

[2] Alemán-Flores, M., Alemán-Flores, P., Álvarez-León, L., Santana-Montesdeoca, J. M., Fuentes-Pavón, P. and Trujillo-Pino, A., (2004) Computational Techniques for the Support of Breast Tumor: Diagnosis on Ultrasound Images, *Instituto Universitario de Ciencias y Tecnologías Cibernéticas*.

[3] R. P. Araujo and D. L. S. McElwain, *A history of the study of solid tumour growth: the contribution of mathematical modelling*, Bull. Math. Biol. **66** (2004), no. 5, 1039–1091, DOI 10.1016/j.bulm.2003.11.002. MR2253816 (2007d:92008)

[4] Hamilton Bueno, Grey Ercole, and Antônio Zumpano, *Asymptotic behaviour of quasi-stationary solutions of a nonlinear problem modelling the growth of tumours*, Nonlinearity **18** (2005), no. 4, 1629–1642, DOI 10.1088/0951-7715/18/4/011. MR2150346 (2006k:35145)

[5] Helen M. Byrne, *A weakly nonlinear analysis of a model of avascular solid tumour growth*, J. Math. Biol. **39** (1999), no. 1, 59–89, DOI 10.1007/s002850050163. MR1705626 (2000i:92011)

[6] Helen Byrne, *Using mathematics to study solid tumour growth*, European women in mathematics (Loccum, 1999), Hindawi Publ. Corp., Cairo, 2000, pp. 81–107. MR1882540

[7] Byrne, H. M. (2010) Dissecting cancer through mathematics: from the cell to the animal model, *Nature Reviews Cancer*, **10** (3): 221–230.

[8] Byrne, H. M. (2012) Mathematical biomedicine and modeling avascular tumor growth, De Gruyter.

[9] Byrne, H. M., Alarcón, T. and Maini, P. K. (2005) Cancer modelling: Getting to the heart of the problem, *Journal of Physiology*, **561**: 4pp.

[10] Byrne, H. M. and Chaplain, M. A. J. (1996) Modelling the role of cell-cell adhesion in the growth and development of carcinomas, *Mathematical and Computer Modelling*, **24**: 1–17.

[11] Byrne, H. M. and Chaplain, M. A. J. (1998) Necrosis and apoptosis: distinct cell loss mechanisms?, *Journal of Theoretical Medicine*, **1**: 223–236.

[12] Byrne, H. M., Owen, M. R., Alarcón, T. and Maini, P. K. (2006a) Cancer disease: integrative modelling approaches, *Proceedings of the 3rd IEEE International Symposium on Biomedical Imaging: Nano to Macro*, IEEE, 806–809.

[13] Helen M. Byrne, Markus R. Owen, Tomas Alarcon, James Murphy, and Philip K. Maini, *Modelling the response of vascular tumours to chemotherapy: a multiscale approach*, Math. Models Methods Appl. Sci. **16** (2006), no. 7, suppl., 1219–1241, DOI 10.1142/S0218202506001522. MR2250126

[14] Byrne, H. M. and Preziosi, L. (2003) Modelling solid tumour growth using the theory of mixtures, *IMA Mathematical Medicine and Biology*, **20** (4): 341–366.

[15] Chaplain, M. A. J. (1993) *The development of a spatial pattern in a model for cancer growth. Experimental and Theoretical Advances in Biological Pattern Formation* (H. G. Othmer, P. K. Maini & J. D. Murray, eds.), Plenum Press, 45–60.

[16] Conger, A. D. and Ziskin, M. C. (1983) Growth of mammalian multicellular tumour spheroids, *Cancer Research*, **43**: 558–60.

[17] Connor, A. J., Cooper, J., Byrne, H. M., Maini, P. K and McKeever, S. (2012) Object-oriented paradigms for modelling vascular tumour growth: a case study, *Proceedings of The Fourth International Conference on Advances in System Simulation, SIMUL 2012*, 74–83.

[18] Vittorio Cristini, John Lowengrub, and Qing Nie, *Nonlinear simulation of tumor growth*, J. Math. Biol. **46** (2003), no. 3, 191–224, DOI 10.1007/s00285-002-0174-6. MR1968541 (2004c:92003)

[19] George Dassios, *Ellipsoidal harmonics*, Theory and applications, Encyclopedia of Mathematics and its Applications, vol. 146, Cambridge University Press, Cambridge, 2012. MR2977792

[20] George Dassios, *On the Young-Laplace relation and the evolution of a perturbed ellipsoid*, Quart. Appl. Math. **72** (2014), no. 1, 21–32, DOI 10.1090/S0033-569X-2013-01321-7. MR3185130

[21] G. Dassios, F. Kariotou, M. N. Tsampas, and B. D. Sleeman, *Mathematical modelling of avascular ellipsoidal tumour growth*, Quart. Appl. Math. **70** (2012), no. 1, 1–24, DOI 10.1090/S0033-569X-2011-01240-2. MR2920612 (2012m:92047)

[22] Feldman, J. P., Goldwasser, R., Mark, S., Schwartz, J. and Orion, I. (2009) A mathematical model for tumor volume evaluation using two-dimensions, *Journal of Applied Quantitative Methods*, **4**: 455–462.

[23] Folkman, J. (1971) Tumour angiogenesis: Therapeutic implications, *New England Journal of Medicine*, **285**: 1182–1186.

[24] Folkman, J. (1972) Anti-angiogenesis: new concept for therapy of solid tumors, *Annals of Surgery*, **175**(3): 409.

[25] Folkman, J. and Hochberg, M. (1973) Self-regulation of growth in three dimensions, *Experimental Medicine*, **138**: 745-753.

[26] Folkman, J., Merler, E., Abernathy, C. and Williams, G. (1971) Isolation of a tumor factor responsible for angiogenesis, *The Journal of Experimental Medicine*, **133**(2):275–288.

[27] Freyer, J. P. (1988) Role of necrosis in regulating the growth saturation of multicell spheroids, *Cancer Research*, **48**: 2432–2439.

[28] Freyer, J. P. and Schor, P. L. (1987) Regrowth of cells from multicell tumour spheroids, *Cell and Tissue Kinetics*, **20**: 249.

[29] Freyer, J. P. and Sutherland, R. M. (1986) Regulation of growth saturation and development of necrosis in EMT6/RO multicellular spheroids glucose and oxygen supply, *Cancer Research*, **46**: 3504–3512.

[30] Greenspan, H. P. (1972) Models for the growth of a solid tumor by diffusion, *Studies in Applied Mathematics*, **51** (4): 317–340.

[31] H. P. Greenspan, *On the growth and stability of cell cultures and solid tumors*, J. Theoret. Biol. **56** (1976), no. 1, 229–242. MR0429164 (55 #2183)

[32] Haji-Karim, M. and Carlsson, J. (1978) Proliferation and viability in cellular spheroids of human origin, *Cancer Research*, **38**:1457–1464.

[33] Inch, W. R., McCredie, J. A. and Sutherland, R. M. (1970) Growth of modular carcinomas in rodents compared with multicell spheroids in tissue culture, *Growth*, **34**: 271–282.

[34] D. S. Jones, M. J. Plank, and B. D. Sleeman, *Differential equations and mathematical biology*, Chapman & Hall/CRC Mathematical and Computational Biology Series, CRC Press, Boca Raton, FL, 2010. Second edition [of MR1967145]. MR2573923

[35] Landry, J., Freyer, J. P. and Sutherland, R. M. (1981) Shedding of mitotic cells from the surface of multicell spheroids during growth, *Journal of Cellular Physiology*, **106**: 23–32.

[36] Leenders, W. P., Kusters, B. and de Waal, R. M. (2002) Vessel co-option: how tumours obtain blood supply in the absence of sprouting angiogenesis, *Endothelium*, **9**(2): 83–87.

[37] Maini, P. K., Alarcón, T. and Byrne, H. M. (2006) Modelling aspects of vascular cancer development, *Proceedings of the International Symposium on Mathematical and Computational Biology*, RP Mondaini and R. Dilao (eds.), World Scientific: 1–12.

[38] Mayr, N. A., Taoka, T., Yuh, W. T. C., Denning, L. M., Zhen, W. K., Paulino, A. C., Gaston, R. C., Sorosky, J. I., Meeks, S. L., Walker, J. L., Mannel, R. S. and Buatti, J. M. (2002) Method and timing of tumor volume measurement for outcome prediction in cervical cancer using magnetic resonance imaging, *International Journal of Radiation Oncology* Biology* Physics*, **52** (1): 14–22.

[39] Mills, K. L., Kemkemer, R., Rudraraju, S, and Garikipati, K. (2014) Elastic FREE energy drives the shape of prevascular solid tumors, *preprint arXiv:1405.3293*.

[40] Markus R. Owen, Tomás Alarcón, Philip K. Maini, and Helen M. Byrne, *Angiogenesis and vascular remodelling in normal and cancerous tissues*, J. Math. Biol. **58** (2009), no. 4-5, 689–721, DOI 10.1007/s00285-008-0213-z. MR2471307 (2010c:92051)

[41] Panovska, J., Byrne, H. M. and Maini, P. K. Mathematical modelling of vascular tumour growth and implications for therapy, *Mathematical Modeling of Biological Systems, Volume I*: 205–216.

[42] Perfahl, H., Byrne, H. M., Chen, T., Estrella, V., Alarcón, T., Lapin, A., Gatenby, R. A., Gillies, R. J., Lloyd, M. C., Maini, P. K., Reuss, M. and Owen, M. R. (2011) Multiscale modelling of vascular tumour growth in 3D: the roles of domain size and boundary conditions, *Public Library of Science One*, **6** (4): e14790.

[43] Luigi Preziosi, ed., *Cancer modelling and simulation*, Chapman & Hall/CRC Mathematical Biology and Medicine Series, Chapman & Hall/CRC, Boca Raton, FL, 2003. MR2005054 (2004d:92007)

[44] Tiina Roose, S. Jonathan Chapman, and Philip K. Maini, *Mathematical models of avascular tumor growth*, SIAM Rev. **49** (2007), no. 2, 179–208, DOI 10.1137/S0036144504446291. MR2327053 (2008d:92013)

[45] SUTHERLAND, R. M. AND DURAND, R. E. (1984) Growth and cellular characteristics of multicell spheroids, *Recent Results in Cancer Research*, **95**: 24–49.
[46] THOMLINSON, R. H. AND GRAY, L. H. (1955) Histological structure of some human lung cancers and the possible implications for radiotherapy, *British Journal of Cancer*, **9**: 539–549.
[47] TRACQUI, P. (2009) Biophysical models of tumor growth, *Reports on Progress in Physics*, **72**.
[48] VAUPEL, P. W., FRINAK, S. AND BICHER, H. I. (1981) Heterogenous oxygen partial pressure and pH distribution in C3H mouse mammary adenocarcinoma, *Cancer Research*, **41**: 2008–2013.
[49] WARD, J. P. AND KING, J. R. (1997) Mathematical modelling of avascular-tumour growth, *IAM Journal of Mathematics Applied in Medicine and Biology*, **14**: 39–69.
[50] WAPNIR, I. L., WARTENBERG, D. E. AND GRECO, R. S. (1996) Three dimensional staging of breast cancer, *Breast cancer research and treatment*, **41** (1):15–19.